

RSNet: A Light Framework for The Detection of SAR Ship Detection

Hongyu Chen[✉], Chengcheng Chen[✉], *Graduate Student Member, IEEE*, Fei Wang[✉],
Yuhu Shi[✉], and Weiming Zeng[✉], *Senior Member, IEEE*

Abstract—Recent advancements in synthetic aperture radar (SAR) ship detection using deep learning have significantly improved accuracy and speed, yet effectively detecting small objects in complex backgrounds with fewer parameters remains a challenge. This letter introduces RSNet, a lightweight framework constructed to enhance ship detection in SAR imagery. To ensure accuracy with fewer parameters, we proposed Waveletpool-ContextGuided (WCG) as its backbone, guiding global context understanding through multi-scale wavelet features for effective detection in complex scenes. Additionally, Waveletpool-StarFusion (WSF) is introduced as the neck, employing a residual wavelet element-wise multiplication structure to achieve higher dimensional nonlinear features without increasing network width. The Lightweight-Shared (LS) module is designed as detect components to achieve efficient detection through lightweight shared convolutional structure and multi-format compatibility. Experiments on the SAR Ship Detection Dataset (SSDD) and High-Resolution SAR Image Dataset (HRSID) demonstrate that RSNet achieves a strong balance between lightweight design and detection performance, surpassing many state-of-the-art detectors, reaching 72.5% and 67.6% in mAP_{.50:.95} respectively with 1.49M parameters. Our code will be released soon.

Index Terms—synthetic aperture radar (SAR), target detection, lightweight model, multiscale feature fusion

I. INTRODUCTION

SYNTHETIC Aperture Radar (SAR) imagery is a vital tool in remote sensing [1], offering high-resolution images under all weather and lighting conditions. By using microwave signals that can penetrate atmospheric obstacles like clouds and rain, SAR provides detailed insights into terrain [2], vegetation [3], and man-made structures [4]. Its applications span geological exploration [5], disaster monitoring [6], agriculture [7], and urban planning. Notably, SAR excels in ocean monitoring [8], detecting subtle surface deformations, and generating digital elevation models, making it indispensable for modern earth observation.

With SAR image data scale and complexity increasing, traditional image processing methods are becoming insufficient [9]. Recent advances in convolutional neural networks (CNNs)

and Transformer architectures have significantly improved target detection [10], [11], [12], [13]. These deep learning methods are generally categorized into candidate region-based and regression-based approaches, with the latter excelling in real-time detection by directly regressing targets at multiple scales. For SAR object detection, one-stage methods strike a promising balance between speed and accuracy; however, due to the computational and energy limitations of airborne platforms, a lightweight model framework is essential for practical deployment.

Building on the established model framework, several notable improvements have been proposed. For example, Tian et al. [14] introduced LFER-Net, which integrates SPDConv and InceptionDWConv for high accuracy and efficiency. Zhou et al. [15] proposed HRLE-SARDet, leveraging hybrid representation learning to improve speed-accuracy balance. Chang et al. [16] presented MLSDNet, utilizing Adaptive Scale Distribution Attention (ASA) to enhance generalization and detection precision. Feng et al. [17] developed LPEDet, an anchor-free SAR ship detection model with a novel position-enhanced attention strategy. Yang et al. [18] designed a lightweight network featuring bidirectional pyramidal structures and soft quantization to minimize accuracy loss and background interference.

While advancements have shown the viability of lightweight models for SAR detection, substantial improvement opportunities remain. SAR images, unlike optical images, are prone to speckle noise, which reduces detail resolution [1], and face increased interpretation complexity due to geometric distortions. Furthermore, the processing of grayscale SAR data lacks intuitive color information. These factors hinder the balance between accuracy and detection speed, particularly regarding the crucial metric mAP_{.50:.95} for optimizing detection performance.

To tackle challenges in remote sensing image detection, we present RSNet (Restar the Sky Network), an optimized network based on YOLOv8, featuring improvements to its backbone, neck, and head. The backbone incorporates the Waveletpool-ContextGuided (WCG) structure, while the head employs the Waveletpool-StarFusion (WSF) network. Additionally, a Lightweight-Shared (LS) module in the detection head reduces the model's parameter load.

The primary contributions of this article are as follows:

- We developed the WCG architecture, enhancing detection accuracy through anti-aliasing and contextual integration, achieving superior performance with fewer parameters.

This work was supported by the National Natural Science Foundation of China (grant nos. 31870979), in part by the 2023 Graduate Top Innovative Talents Training Program at Shanghai Maritime University under Grant 2023YBR013. (Corresponding author: Weiming Zeng)

Hongyu Chen, Chengcheng Chen, Fei Wang, Yuhu Shi, Weiming Zeng are with the Laboratory of Digital Image and Intelligent Computation, Shanghai Maritime University, Shanghai 201306, China (e-mail: hongychen676@gmail.com, shmtu_ccc@163.com, shine_wxf@163.com, syhustb2011@163.com, zengwm86@163.com).

Manuscript received XX, XXXX; revised XXXX XX, XXXX.

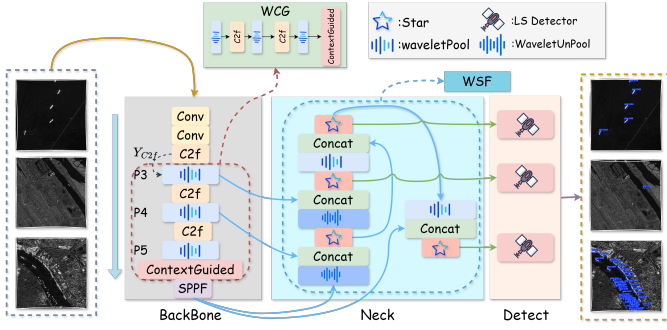


Fig. 1: Overall flow of the RSNet.

- The WSG network is constructed by combining wavelet upsampling pooling and element-wise multiplication through the residual structure, significantly reducing parameters while maintaining computational efficiency.
- We introduced the LS module using the group normalization strategy to further minimize the parameter burden of the detection head, thereby enhancing the overall efficiency of RSNet.
- Experiments conducted on the SSDD and the HRSID show that the proposed RSNet strikes an improved balance between lightweight design and detection performance.

II. PROPOSED METHOD

A. Overall Architecture

This letter introduces RSNet (Restar the Sky Network), a lightweight network for ship detection in SAR images, structured into backbone, neck, and detect components as illustrated in Fig. 1. The backbone processes the input image through the first three layers to produce feature maps, which is then enhanced by multiple scales of wavelet pooling to generate multi-scale feature maps. The ContextGuided block further enriches feature extraction by integrating contextual information. In the neck, the WSG module employs wavelet upsampling to restore spatial resolution and fuse features. The lightweight star module combines an element-wise multiplication structure with skip connections for deeper feature extraction, enhancing small object recognition capability. Finally, the LS Detector module connects the features to output the bounding boxes, class labels, and confidence scores of the detected objects.

B. Waveletpool-ContextGuided (WCG)

In complex backgrounds, including land structures, clutter, and coastlines, current SAR ship detectors face challenges in accurately locating ships. To achieve better performance with fewer parameters, this letter proposes WCG.

The WCG network introduces a wavelet pooling mechanism that efficiently extracts multi-scale spatial features, reducing computational complexity while enhancing sensitivity to subtle details in complex backgrounds. This allows the network to focus on potential ship targets in noisy environments. Additionally, the context guided convolutional module integrates surrounding environmental information, significantly

improving detection of small targets, especially in high-noise conditions. By leveraging contextual information, the model better distinguishes real ship targets from background noise, enhancing localization accuracy. Below are specific descriptions of wavelet pooling and context guided convolution.

1) *Wavelet Pooling*: In the WCG, the WaveletPool module plays a critical role, designed to effectively extract multi-scale features from the input feature map through wavelet transforms. The output Y_{pool} of this module is defined by the following formula:

$$Y_{pool} = Conv_{2D}(Y_{C2f}) \in R^{B \times C_{out} \times H \times W}, \quad (1)$$

where we define the output feature map from C2f as Y_{C2f} . B is the batch size. H and W are the dimensions of the downsampled output. C_{out} is the number of output channels of the WaveletPool block. The filter set F used in the WaveletPool operation consists of four different convolutional kernels defined as:

$$F = \{F_{LL}, F_{LH}, F_{HL}, F_{HH}\},$$

$$F_{LL} = \begin{bmatrix} 0.5 & 0.5 \\ 0.5 & 0.5 \end{bmatrix}, F_{LH} = \begin{bmatrix} -0.5 & -0.5 \\ 0.5 & 0.5 \end{bmatrix}, \quad (2)$$

$$F_{HL} = \begin{bmatrix} -0.5 & 0.5 \\ -0.5 & 0.5 \end{bmatrix}, F_{HH} = \begin{bmatrix} 0.5 & -0.5 \\ -0.5 & 0.5 \end{bmatrix},$$

where F_{LL} is equivalent to average pooling. The WaveletPool operation can be expressed as:

$$Y_{pool} = \sum_{j=1}^4 F_j * Y_{C2f}, \quad (3)$$

where $*$ denotes the convolution operation. This operation extracts multi-scale features from the input feature map by applying each filter F_j and aggregating the results across the channel dimension.

2) *Context Guided*: The ContextGuided block takes the input feature map and performs a series of operations, defined as:

$$Y_{CGB} = CGB(Y_{pool}). \quad (4)$$

The processing steps within the ContextGuided block can be expressed as follows:

$$X_1 = Conv_{1 \times 1}(Y_{pool}) \in R^{B \times n \times H \times W}, n = \frac{C_{out}}{2}, \quad (5)$$

where n represents the number of the input channels. Then a depthwise convolution is employed to capture local features L , and another depthwise convolution with a dilation rate d is applied to capture the surrounding features S :

$$L = Conv_{3 \times 3}(X_1) \in R^{B \times n \times H \times W}, \quad (6)$$

$$S = Conv_{3 \times 3}(X_1) \text{ with dilation rate } d. \quad (7)$$

The L and S are concatenated, normalized, and activated, generating the global context feature F_{glo} through the global feature extraction module:

$$J = BatchNorm(Concat(L, S)) \in R^{B \times 2n \times H \times W}, \quad (8)$$

$$G = F_{glo}(J) \in R^{B \times C_{out} \times H \times W}. \quad (9)$$

Finally, the output of the Context Guided Block is computed by adding the input to the global context refinement output:

$$Y_{CGB} = Y_{pool} + G. \quad (10)$$

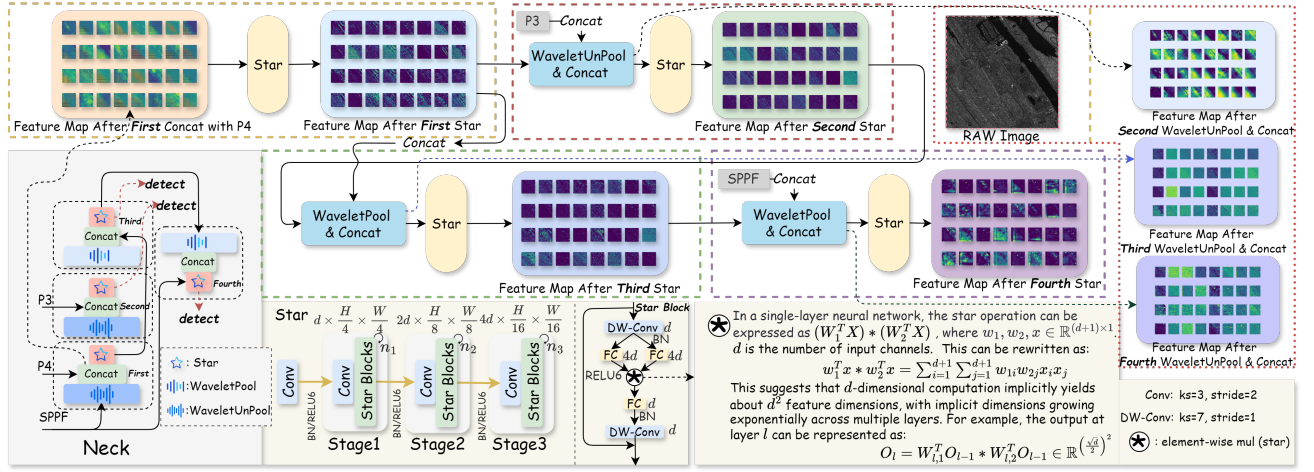


Fig. 2: Flowchart of WSF (Neck of RSNet). The feature map from the backbone network is processed by a residual structure comprising four submodules: WaveletUnPool, Concat, and Star. The network structure of the Star module is also illustrated.

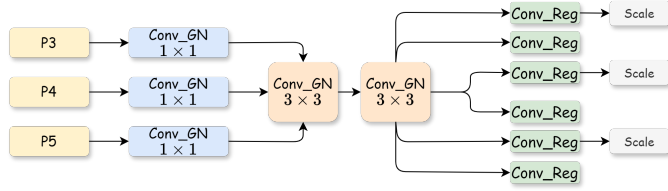


Fig. 3: The structure of LS Detector.

C. Waveletpool-StarFusion (WSF)

Although the WCG module reduces parameters, this letter proposes WSF to better balance parameters and model accuracy as described in Fig. 2. WaveletUnPool and Star module enhance SAR ship detection by restoring spatial resolution and retaining rich features for improved contour recognition. Star module utilizes depthwise separable convolutions and element-wise multiplication operations for real-time applicability while effectively mitigating noise. Together, they significantly enhance performance and efficiency in ship detection.

1) *WaveletUnPool*: WaveletUnPool, in contrast, aims to restore the spatial resolution of the downsampled feature map, effectively reconstructing its original dimensions. It utilizes transpose convolution with a stride of 2, employing the same wavelet filters as described in formula 2 to upsample the feature map back to a higher resolution.

2) *Star*: Element-wise multiplication structure inside Star-Net [19] which is an advanced deep learning architecture that enhances model representation. By fusing features from different subspaces with element-wise multiplication at each layer, it expands implicit feature dimensions without significantly increasing parameters. Fig. 2 illustrates this process in the neck section, showing the initial concatenation of the feature map before inputting it into Star module, along with the computational flow involved.

The calculation process of Star block is explained below. The Star block receives an input feature map x_{in} with di-

mensions $C \times H' \times W'$, where C is the number of channels, and H' and W' are the height and width of the feature map, respectively.

- First, a depthwise convolution is applied to the input feature map x_{in} , and W_k is the convolution kernel for the k -th channel:

$$x_{in}' = DWConv(x_{in}) = \sum_{k=1}^C W_k * x_{in}, \quad (11)$$

- Next, 1×1 convolution layers are used to transform features, producing two feature maps:

$$\begin{aligned} x_1' &= Conv_{1 \times 1}(x_{in}') = W_1 \cdot x_{in}' + b_1, \\ x_2' &= Conv_{1 \times 1}(x_{in}') = W_2 \cdot x_{in}' + b_2. \end{aligned} \quad (12)$$

- Then, the first feature map undergoes ReLU6 activation, followed by element-wise multiplication with the second feature map x_{in}'' , and another another 1×1 convolution layer is applied to generate a new feature map $x^{(new)}$:

$$x_{in}'' = \min(\max(0, x_1'), 6) \odot x_2', \quad (13)$$

$$\begin{aligned} x^{(new)} &= DWConv2(Conv_{1 \times 1}(g(x_{in}''))) \\ &= \sum_{k=1}^C W_k^{new} * g(x_{in}''). \end{aligned} \quad (14)$$

- Finally, a residual connection is established by adding the input feature map x_{in} to the newly generated feature map, applying dropout for regularization:

$$y = x_{in} + \text{dropout}(x^{(new)}) \quad (15)$$

D. LS Detector

The FOCS [20] shows that groupnorm enhances detection head performance in localization and classification. Shared convolutions reduce model parameters, facilitating lightweight design for resource-constrained devices. To address inconsistencies in handling targets of varying scales, we introduce a scale layer for feature adjustment. The specific structure is shown in Fig. 3. These strategies lower parameters and computational load while maintaining accuracy.

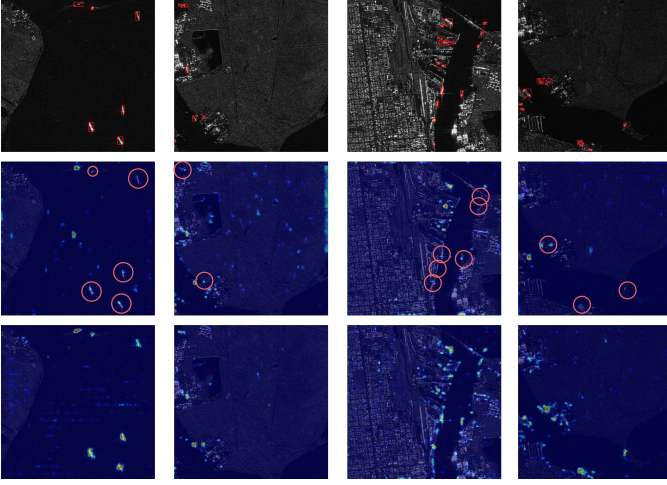


Fig. 4: The heat-map visualization results feature three rows: the first row illustrates the ground truth, the second row presents the baseline1 (YOLOv8n), and the third row highlights our proposed method. Red circles represent missed detections.

TABLE I: SPECIFIC EXPERIMENTAL DETAILS

Dataset	Epochs	Optimizer	Batch	Lr0	Momentum	Weight_decay
SSDD	300	AdamW	16	0.002	0.937	5e-4
HRSID	300	AdamW	16	0.002	0.937	5e-4

III. EXPERIMENT

A. Datasets

We evaluated our model on two public SAR datasets: SSDD [21] and HRSID [22]. SSDD includes 1160 images, with 928 for training and 232 for testing as per the original split. HRSID follows the official split, using 3642 training and 1962 testing images.

B. Training Details

Our experiments were conducted on a system running Ubuntu 20.04, equipped with an Intel Xeon Silver 4210R CPU and a Nvidia GeForce Tesla V100 16G. And the image size is set to 640. The specific experimental details are shown in Table I.

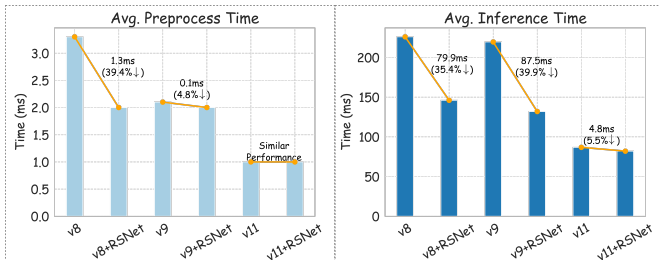


Fig. 5: Performance Comparison of Three Baseline Models and the RSNet-Enhanced Model in Terms of Preprocessing Time and Inference Time.

TABLE II: ABLATION EXPERIMENTS ON HRSID

Baseline1 (YOLOv8n)						
WCG	WSF	LS	mAP _{.50} (%)	mAP _{.50:.95} (%)	Params(M)	FLOPs(G)
×	×	×	91.1	66.9	3.01	8.1
✓	×	×	91.2 (0.6 ↑)	66.5 (0.4 ↓)	2.43 (0.58 ↓)	7.4 (0.7 ↓)
✓	✓	×	91.1	65.8 (1.1 ↓)	2.13 (0.88 ↓)	6.8 (1.3 ↓)
✓	✓	✓	91.2 (0.1 ↑)	67.6 (0.7 ↑)	1.49 (1.52 ↓)	5.1 (3.0 ↑)
Baseline2 (YOLOv9n)						
WCG	WSF	LS	mAP _{.50} (%)	mAP _{.50:.95} (%)	Params(M)	FLOPs(G)
×	×	×	90.5	66.1	2.01	7.8
✓	×	×	91.1 (0.6 ↑)	66.9 (0.8 ↑)	1.65 (0.36 ↓)	7.2 (0.6 ↓)
✓	✓	×	90.3 (0.2 ↓)	65.6 (0.5 ↓)	1.24 (0.77 ↓)	5.9 (1.9 ↓)
✓	✓	✓	91.1 (0.6 ↑)	66.6 (0.5 ↑)	0.77 (1.24 ↓)	4.5 (3.3 ↓)
Baseline3 (YOLOv11n)						
WCG	WSF	LS	mAP _{.50} (%)	mAP _{.50:.95} (%)	Params(M)	FLOPs(G)
×	×	×	89.7	65.8	2.59	6.4
✓	×	×	90.0 (0.3 ↑)	66.2 (0.4 ↑)	2.01 (0.58 ↓)	5.2 (1.2 ↓)
✓	✓	×	90.0 (0.3 ↑)	66.1 (0.3 ↑)	1.30 (1.29 ↓)	5.1 (1.3 ↓)
✓	✓	✓	91.1 (0.4 ↑)	67.0 (1.2 ↑)	1.05 (1.54 ↓)	4.9 (1.5 ↓)

TABLE III: COMPARISON EXPERIMENTS ON HRSID

Method	mAP _{.50} (%)	mAP _{.50:.95} (%)	Params(M)	FLOPs(G)
Faster R-CNN-FPN	72.0	46.5	41.35	134
RetinaNet [20]	78.9	53.6	36.33	128
YOLOv6n [23]	88.2	62.8	4.23	11.8
YOLOv7-tiny [24]	85.4	57.2	6.01	13.2
YOLOv8n	91.1	66.9	3.01	8.1
YOLOv9t [25]	90.5	66.1	2.01	7.8
YOLOv10n [26]	89.6	66.3	2.71	8.4
YOLOv11n	89.7	65.8	2.59	6.4
YOLOv12n [27]	85.4	60.7	2.52	6.0
Yue et al. [28]*	91.1	66.5	43.42	-
CPoints-Net [29]*	90.5	-	18.64	102.2
FEPS-Net [30]*	90.7	65.7	37.31	-
BL-Net [31]*	88.67	-	47.81	-
FBUA-Net [32]*	90.3	-	36.54	-
CS ⁿ Net [33]*	91.2	60.6	12.2	21.7
Ours (YOLOv8n-based)	91.2	67.6	1.49	5.1

* Denotes data obtained from their papers

C. Evaluation Metrics

Model performance was assessed using mAP_{.50} and mAP_{.50:.95} for detection accuracy, alongside parameter count (Params) and FLOPs to quantify model complexity and computational efficiency.

D. Ablation Experiments

To validate the module's effectiveness, we conducted ablation experiments on the HRSID dataset based on YOLOv8n, YOLOv9n and YOLOv11n, as shown in Table II. We also performed feature visualization experiments, illustrated in Fig.

TABLE IV: COMPARISON EXPERIMENTS ON SSDD

Method	mAP _{.50} (%)	mAP _{.50:.95} (%)	Params(M)	FLOPs(G)
Faster R-CNN-FPN	94.0	64.0	41.35	134
RetinaNet [20]	90.2	60.0	36.33	128
YOLOv6n [23]	96.9	71.2	4.23	11.8
YOLOv7-tiny [24]	96.4	66.5	6.01	13.2
YOLOv8n	98.2	73.1	3.01	8.1
YOLOv9t [25]	98.2	71.2	2.01	7.8
YOLOv10n [26]	97.0	71.3	2.71	8.4
YOLOv11n	98.0	72.0	2.59	6.4
YOLOv12n [27]	97.3	70.1	2.52	6.0
Yue et al. [28]*	95.7	64.8	43.42	-
CPoints-Net [29]*	96.3	-	18.64	102.2
FEPS-Net [30]*	96.0	73.1	37.31	-
BL-Net [31]*	95.25	-	47.81	-
FBUA-Net [32]*	96.2	-	36.54	-
CS ⁿ Net [33]*	97.1	64.9	12.2	21.7
Ours (YOLOv8n-based)	98.4	72.5	1.49	5.1

* Denotes data obtained from their papers

4, which demonstrate that our model effectively identifies real targets while reducing the influence of surrounding noise. To evaluate the performance of the proposed framework under computational constraints, we test the baseline models and their RSNet-enhanced models on an Intel i5-8265U CPU (TDP = 15W) at 20°C under CPU-only inference for fair comparison. Results are shown in Fig. 5.

E. Comparison Experiments

We selected several representative object detectors, including the classic two-stage Faster R-CNN-FPN [34], one-stage RetinaNet [20], and YOLOv6n [23], YOLOv7-tiny [24], YOLOv8n and YOLOv11n. Additionally, we compared algorithms specifically designed for target detection in SAR images. The experimental results, presented in Tables III and IV, demonstrate that our method effectively balances parameter quantity and performance, outperforming other methods.

IV. CONCLUSIONS

This letter introduces RSNet, a lightweight network for SAR ship detection that enhances accuracy and efficiency through its innovative architecture. The WCG backbone improves performance with fewer parameters, facilitating effective feature extraction and context understanding. The WSF neck optimizes feature integration, while the LS module ensures efficient detection with minimal computational overhead. Future work will explore RSNet's application to other detection tasks and datasets, further expanding its utility in remote sensing.

REFERENCES

- [1] A. Moreira, P. Prats-Iraola, M. Younis, G. Krieger, I. Hajnsek, and K. P. Papathanassiou, "A tutorial on synthetic aperture radar," *IEEE Geosci. Remote Sens. Mag.*, vol. 1, no. 1, pp. 6–43, 2013.
- [2] M. C. Dobson, F. T. Ulaby, and L. E. Pierce, "Land-cover classification and estimation of terrain attributes using synthetic aperture radar," *Remote Sens. Environ.*, vol. 51, no. 1, pp. 199–214, 1995.
- [3] X. Bao, R. Zhang, J. Lv, R. Wu, H. Zhang, J. Chen, B. Zhang, X. Ouyang, and G. Liu, "Vegetation descriptors from sentinel-1 sar data for crop growth monitoring," *ISPRS J. Photogramm. Remote Sens.*, vol. 203, pp. 86–114, 2023.
- [4] P. Connetable, K. Conradsen, A. A. Nielsen, and H. Skriver, "Corrections to "test statistics for reflection symmetry: Applications to quad-polarimetric sar data for detection of man-made structures"," *IEEE J. Sel. Topics Appl. Earth Observ. Remote Sens.*, 2024.
- [5] S. Baraha and A. K. Sahoo, "Synthetic aperture radar image and its despeckling using variational methods: A review of recent trends," *Signal Process.*, vol. 212, p. 109156, 2023.
- [6] S. Karimzadeh, M. Ghasemi, M. Matsuoka, K. Yagi, and A. C. Zulfikar, "A deep learning model for road damage detection after an earthquake based on synthetic aperture radar (sar) and field datasets," *IEEE J. Sel. Topics Appl. Earth Observ. Remote Sens.*, vol. 15, pp. 5753–5765, 2022.
- [7] M. G. Hashemi, E. Jalilvand, H. Alemohammad, P.-N. Tan, and N. N. Das, "Review of synthetic aperture radar with deep learning in agricultural applications," *ISPRS J. Photogramm. Remote Sens.*, vol. 218, pp. 20–49, 2024.
- [8] R. M. Asiyabi, A. Ghorbanian, S. N. Tameh, M. Amani, S. Jin, and A. Mohammadzadeh, "Synthetic aperture radar (sar) for ocean: A review," *IEEE J. Sel. Topics Appl. Earth Observ. Remote Sens.*, 2023.
- [9] G. Fracastoro, E. Magli, G. Poggi, G. Scarpa, D. Valsesia, and L. Verdoliva, "Deep learning methods for synthetic aperture radar image despeckling: An overview of trends and perspectives," *IEEE Geosci. Remote Sens. Mag.*, vol. 9, no. 2, pp. 29–51, 2021.
- [10] F. Wang, C. Chen, and W. Zeng, "Hybrid multi-scale sar ship detector with cnn-transformer and adaptive fusion loss," *IEEE Geosci. Remote Sens. Lett.*, 2024.
- [11] L. Du, L. Li, Y. Guo, Y. Wang, K. Ren, and J. Chen, "Two-stream deep fusion network based on vae and cnn for synthetic aperture radar target recognition," *Remote Sens.*, vol. 13, no. 20, p. 4021, 2021.
- [12] X. Zhang, S. Feng, C. Zhao, Z. Sun, S. Zhang, and K. Ji, "Mgsfa-net: Multi-scale global scattering feature association network for sar ship target recognition," *IEEE J. Sel. Topics Appl. Earth Observ. Remote Sens.*, 2024.
- [13] J. Shen, L. Bai, Y. Zhang, M. C. Momi, S. Quan, and Z. Ye, "Ellk-net: An efficient lightweight large kernel network for sar ship detection," *IEEE Trans. Pattern Anal. Mach. Intell.*, 2024.
- [14] C. Tian, D. Liu, F. Xue, Z. Lv, and X. Wu, "Faster and lighter: A novel ship detector for sar images," *IEEE Geosci. Remote Sens. Lett.*, 2024.
- [15] Z. Zhou, J. Chen, Z. Huang, J. Lv, J. Song, H. Luo, B. Wu, Y. Li, and P. S. Diniz, "Hrle-sardet: A lightweight sar target detection algorithm based on hybrid representation learning enhancement," *IEEE Trans. Geosci. Remote Sens.*, vol. 61, pp. 1–22, 2023.
- [16] H. Chang, X. Fu, J. Dong, J. Liu, and Z. Zhou, "Mlsdnet: Multi-class lightweight sar detection network based on adaptive scale distribution attention," *IEEE Geosci. Remote Sens. Lett.*, 2023.
- [17] Y. Feng, J. Chen, Z. Huang, H. Wan, R. Xia, B. Wu, L. Sun, and M. Xing, "A lightweight position-enhanced anchor-free algorithm for sar ship detection," *Remote Sens.*, vol. 14, no. 8, p. 1908, 2022.
- [18] X. Yang, J. Zhang, C. Chen, and D. Yang, "An efficient and lightweight cnn model with soft quantification for ship detection in sar images," *IEEE Trans. Geosci. Remote Sens.*, vol. 60, pp. 1–13, 2022.
- [19] X. Ma, X. Dai, Y. Bai, Y. Wang, and Y. Fu, "Rewrite the stars," in *Proc. IEEE/CVF Conf. Comput. Vis. Pattern Recognit. (CVPR)*, 2024, pp. 5694–5703.
- [20] T. Lin, "Focal loss for dense object detection," *arXiv preprint arXiv:1708.02002*, 2017.
- [21] T. Zhang, X. Zhang, J. Li, X. Xu, B. Wang, X. Zhan, Y. Xu, X. Ke, T. Zeng, H. Su *et al.*, "Sar ship detection dataset (ssdd): Official release and comprehensive data analysis," *Remote Sens.*, vol. 13, no. 18, p. 3690, 2021.
- [22] S. Wei, X. Zeng, Q. Qu, M. Wang, H. Su, and J. Shi, "Hrsid: A high-resolution sar images dataset for ship detection and instance segmentation," *Ieee Access*, vol. 8, pp. 120 234–120 254, 2020.
- [23] C. Li, L. Li, H. Jiang, K. Weng, Y. Geng, L. Li, Z. Ke, Q. Li, M. Cheng, W. Nie *et al.*, "Yolov6: A single-stage object detection framework for industrial applications," *arXiv preprint arXiv:2209.02976*, 2022.
- [24] C.-Y. Wang, A. Bochkovskiy, and H.-Y. M. Liao, "Yolov7: Trainable bag-of-freebies sets new state-of-the-art for real-time object detectors," in *Proc. IEEE/CVF Conf. Comput. Vis. Pattern Recognit. (CVPR)*, 2023, pp. 7464–7475.
- [25] C.-Y. Wang, I.-H. Yeh, and H.-Y. Mark Liao, "Yolov9: Learning what you want to learn using programmable gradient information," in *Proc. European Conf. Comput. Vision*. Springer, 2024, pp. 1–21.
- [26] A. Wang, H. Chen, L. Liu, K. Chen, Z. Lin, J. Han, and G. Ding, "Yolov10: Real-time end-to-end object detection. arxiv 2024," *arXiv preprint arXiv:2405.14458*, 2024.
- [27] Y. Tian, Q. Ye, and D. Doermann, "Yolov12: Attention-centric real-time object detectors," *arXiv preprint arXiv:2502.12524*, 2025.
- [28] T. Yue, Y. Zhang, P. Liu, Y. Xu, and C. Yu, "A generating-anchor network for small ship detection in sar images," *IEEE J. Sel. Topics Appl. Earth Observ. Remote Sens.*, vol. 15, pp. 7665–7676, 2022.
- [29] F. Gao, C. Cai, W. Tang, and Y. He, "A compact and high-efficiency anchor-free network based on contour key points for sar ship detection," *IEEE Geosci. Remote Sens. Lett.*, 2024.
- [30] L. Bai, C. Yao, Z. Ye, D. Xue, X. Lin, and M. Hui, "Feature enhancement pyramid and shallow feature reconstruction network for sar ship detection," *IEEE J. Sel. Topics Appl. Earth Observ. Remote Sens.*, vol. 16, pp. 1042–1056, 2023.
- [31] T. Zhang, X. Zhang, C. Liu, J. Shi, S. Wei, I. Ahmad, X. Zhan, Y. Zhou, D. Pan, J. Li *et al.*, "Balance learning for ship detection from synthetic aperture radar remote sensing imagery," *ISPRS J. Photogramm. Remote Sens.*, vol. 182, pp. 190–207, 2021.
- [32] L. Bai, C. Yao, Z. Ye, D. Xue, X. Lin, and M. Hui, "A novel anchor-free detector using global context-guide feature balance pyramid and united attention for sar ship detection," *IEEE Geosci. Remote Sens. Lett.*, vol. 20, pp. 1–5, 2023.
- [33] C. Chen, W. Zeng, X. Zhang, and Y. Zhou, "Cs n net: a remote sensing detection network breaking the second-order limitation of transformers with recursive convolutions," *IEEE Trans. Geosci. Remote Sens.*, 2023.
- [34] S. Ren, K. He, R. Girshick, and J. Sun, "Faster r-cnn: Towards real-time object detection with region proposal networks," *IEEE Trans. Pattern Anal. Mach. Intell.*, vol. 39, no. 6, pp. 1137–1149, 2016.